Physics and Imaging in Radiation Oncology 28 (2023) 100504

Contents lists available at ScienceDirect

Physics and Imaging in Radiation Oncology

journal homepage: www.sciencedirect.com/journal/physics-and-imaging-in-radiation-oncology

Original Research Article

Development of a comprehensive cardiac atlas on a 1.5 Tesla Magnetic Resonance Linear Accelerator

Aronne M. Schottstaedt [a,*], Eric S. Paulson [a,b], Jason C. Rubenstein [b,c], Xinfeng Chen [a], Eenas A. Omari [a], X Allen Li [a], Chris J. Schultz [a], Lindsay L. Puckett [a], Clifford G. Robinson [d], Filippo Alongi [e], Elizabeth M. Gore [a], William A. Hall [a]

[a] Medical College of Wisconsin, Department of Radiation Oncology, Milwaukee, WI, United States
[b] Medical College of Wisconsin, Department of Radiology, Milwaukee, WI, United States
[c] Medical College of Wisconsin, Department of Cardiology, Milwaukee, WI, United States
[d] Washington University, Department of Radiation Oncology, St. Louis, MO, United States
[e] IRCCS Sacro Cuore Don Calabria Hospital, Department of Radiation Oncology, Negrar-Verona, Italy & University of Brescia, Faculty of Medicine, Brescia, Italy

ARTICLE INFO

Keywords:
Radiation Oncology Cardiac Atlas
MRgRT
1.5T MRL
Cardiac conduction system
Contouring guidelines

ABSTRACT

Background and purpose: The 1.5 Tesla (T) Magnetic Resonance Linear Accelerator (MRL) provides an innovative modality for improved cardiac imaging when planning radiation treatment. No MRL based cardiac atlases currently exist, thus, we sought to comprehensively characterize cardiac substructures, including the conduction system, from cardiac images acquired using a 1.5 T MRL and provide contouring guidelines.
Materials and methods: Five volunteers were enrolled in a prospective protocol (NCT03500081) and were imaged on the 1.5 T MRL with Half Fourier Single-Shot Turbo Spin-Echo (HASTE) and 3D Balanced Steady-State Free Precession (bSSFP) sequences in axial, short axis, and vertical long axis. Cardiac anatomy was contoured by (AS) and confirmed by a board certified cardiologist (JR) with expertise in cardiac MR imaging.
Results: A total of five volunteers had images acquired with the HASTE sequence, with 21 contours created on each image. One of these volunteers had additional images obtained with 3D bSSFP sequences in the axial plane and additional images obtained with HASTE sequences in the key cardiac planes. Contouring guidelines were created and outlined. 15–16 contours were made for the short axis and vertical long axis. The cardiac conduction system was demonstrated with eleven representative contours. There was reasonable variation of contour volume across volunteers, with structures more clearly delineated on the 3D bSSFP sequence.
Conclusions: We present a comprehensive cardiac atlas using novel images acquired prospectively on a 1.5 T MRL. This cardiac atlas provides a novel resource for radiation oncologists in delineating cardiac structures for treatment with radiotherapy, with special focus on the cardiac conduction system.

1. Introduction

Radiation oncologists have limited experience with cardiovascular magnetic resonance imaging (CMR). Cardiac substructures impact clinical outcomes following thoracic radiation [1,2]. Cardiac ablation using stereotactic body radiation therapy (SBRT) has tremendous potential [3,4], highlighting the need for an understanding of key conduction structures and contours to guide treatment and research. Furthermore, practices are rapidly adopting MR guided radiation therapy (MRgRT) [5]. These advances require an understanding of basic principles underlying CMR and an atlas of relevant cardiac substructures. However, no CMR atlases designed for radiotherapy exist. Magnetic Resonance Linear Accelerator (MRL) images differ from diagnostic MR images given limitations/differences in optimization between modalities. Thus, an MRL based contouring atlas is needed, especially for future workflows intending to omit CT simulation.

CMR has been widely adopted in cardiac imaging for assessment of ventricular function, cardiovascular morphology, tissue characterization, myocardial perfusion, and flow quantification [6]. Clinically, CMR is utilized to further evaluate myocardial ischemia/infarction, valvular disease, cardiomyopathy, pericardial disease, coronary artery disease, cardiac masses, and congenital anomalies [7]. Functional MR data has

* Corresponding author at: Medical College of Wisconsin, 8701 W Watertown Plank Rd, Milwaukee, WI 53226, United States.
E-mail address: ajschotts40@gmail.com (A.M. Schottstaedt).

https://doi.org/10.1016/j.phro.2023.100504
Received 1 June 2023; Received in revised form 18 October 2023; Accepted 30 October 2023
Available online 7 November 2023

been used to study myocardial structure, cardiac function, vascular blood flow, myocardial perfusion, and myocardial viability [8]. Further, research in CMR is rapidly evolving, with novel sequences under investigation to better visualize left ventricle (LV) function, regional perfusion, angiogenesis, myocardial viability and orientation of myocytes [9].

CMR differs from MR imaging of other body regions due to constant heart motion, respiratory motion, blood flow/pulsation artifacts, and heart orientation [7]. To compensate for cardiac motion, MR images can be gated with the cardiac cycle using EKG to generate a cine image set [8,10]. This image set is generated over multiple heart beats, with different parts of the image generated with each beat [6,8] (Supplementary Figure S1). Cardiac gating can also be coupled with respiratory gating [7]. Alternatively, ultra-fast MR acquisition techniques [6], or advanced MR motion based reconstruction techniques can be employed [11].

Cardiac specific imaging planes are generated to better visualize cardiac structures. The horizontal long axis (four chamber), short axis, and vertical long axis (two chamber) are commonly used in CMR, and are orthogonal planes relative to one another. They are generated relative to the long axis of the heart, i.e. a line drawn from the apex of the LV through the center of the mitral valve [7,12]. If the heart is positioned with the apex pointing at the observer, the LV on the right and right ventricle (RV) on the left, the short axis view is essentially coronal slices of the LV, creating a two chamber view. The horizontal long axis and vertical long axis are similar to axial, creating a four chamber view, and sagittal planes respectively. These have been previously pictorially demonstrated [7,12]. In this cardiac atlas, the axial (transverse) plane is used in place of the horizontal long axis because thoracic imaging, prior atlases, and thoracic radiation treatments have been imaged and planned in the axial plane. It remains to be seen if radiation oncologists adopt cardiac planes for cardiac ablation.

Cardiac radiation exposure is a concern in cancer treatment. The risk of major coronary events increases by 7.4 % per Gy of increased mean heart dose [13]. Dose to the pulmonary artery, coronary arteries, and LV have been related to cardiac outcomes such as cardiac death, valvular disease, pericardial disease, coronary artery stenosis, and ventricular abnormalities [14–25]. Dose to the base of the heart and AV node have been shown to impact overall survival [26]. These insights are being investigated further on the ACCOLADE trial, investigating dose constraints for cardiac substructures in patients treated for lung cancer [27].

The aim of the current study is to provide a 1.5 T MRL based cardiac atlas and set of contouring guidelines to comprehensively characterize cardiac substructures and the conduction system.

2. Materials and methods

Representative images from healthy volunteers at Froedtert and the Medical College of Wisconsin recruited through the IRB approved, prospective, solid tumor imaging MR-Linac (STIM) protocol (NCT03500081) were acquired on a 1.5 T MRL (Unity, Elekta Instruments, AB). Five volunteers had Breath Held Half Acquired Single-Shot Turbo Spin-Echo (HASTE) sequences in the axial plane acquired. One of these volunteers had HASTE sequences acquired in short axis and vertical long axis, and a free-breathing 3D Vane High Resolution with balanced steady-state free precession excitation (3D bSSFP) sequence. Sequence parameters are outlined in Supplementary Table S1. These sequences were chosen for their speed of acquisition and frequent use in CMR, generating quality images without cardiac gating, which is not yet available on the 1.5 T MRL. They represent two common image sets that radiation oncologists will likely use when contouring cardiac structures on the MRL. Images were uploaded in commercially available software (MIM Software Inc, Cleveland, Ohio), where cardiac anatomy was contoured (AS) and confirmed by a board certified cardiologist (JR). Contours were informed by CT based radiation oncology cardiac atlases, CMR atlases, anatomy textbooks, and the University of Minnesota atlas of human cardiac anatomy [28–36]. Representative contours of the electrical conduction system were created on the axial 3D bSSFP images based on identifiable landmarks. Mean and standard deviation contour volumes for each volunteer on each sequence were also reported for reference. These values may not be representative of the readers population of interest, however, given the use of volunteers and not patients with cardiac disease.

3. Results

3.1. Atlas images

Contours of cardiac anatomy and the electrical conduction system were created according to contouring guidelines provided. Unfortunately, limitations in current MRL imaging (coils, magnet strength, lack of cardiac gating, limited number of sequences) limit the ability to directly image the conduction system. Instead, these structures are contoured based on neighboring landmarks to create surrogate contours likely to receive similar dose. Ascending axial 3D bSSFP slices with key cardiac structures are contoured and labeled in Fig. 1. Fig. 2 shows ascending, short axis HASTE slices and Fig. 3 shows ascending, vertical long axis HASTE slices. Fig. 4 shows contours of axial HASTE slices acquired on four different volunteers to better delineate slight variations in normal anatomy. Fig. 5 shows contours of the cardiac conduction system based on neighboring anatomy. Figs. 1-3 and Fig. 5 were all acquired on a single volunteer. For a comprehensive view of acquired images for axial 3D bSSFP and short and vertical long axis HASTE, refer to Supplementary Figure S2-S4.

3.2. Contouring guidelines – Heart chambers

Left ventricle: The leftmost, largest chamber. The anterior border is the pericardium/chest wall, left border is the pericardium/lung, right border is the RV/left ventricular outflow tract (LVOT), and posterior border is the left atrium (LA). The LV contour includes the hypointense surrounding muscular wall (i.e. myocardium) and blood product bounded by this wall, but not the hyperintense surrounding pericardium. The distinction between the LA and LV is an imaginary line drawn from the posterior left most portion of the LVOT, where it meets the LV, to the myocardium, perpendicular to the long axis of the LV. Though not visualized, this line is where the mitral valve resides. The LV ends a slice above (superiorly) and a slice below (inferiorly) where the blood is no longer visualized.

Ventricular outflow tract: Bounded anteriorly by the RV, on the left by the LV, on the right by the RA, and posteriorly by the LA. It begins inferiorly shortly after the RA comes into view, as a posteromedial outpouching of the LV. Superiorly, the LVOT contour becomes the aorta where the structure appears very circular and constant in shape, roughly at the superior extent of the LV contour.

Left atrium: The most posterior chamber. Bounded anteriorly by the LV/RA/LVOT, on the right by the RA/pericardium/lung, on the left by the LV/pericardium/lung, and posteriorly by the esophagus/spinal column/pericardium. The contour ends inferiorly with the LV, as the blood within the LA is no longer visible, and the contour would otherwise overlap with the LV. The contour ends superiorly with blood no longer visualized, just inferior to the bifurcation of the pulmonary trunk (PT).

Right ventricle: The most anterior chamber. Bounded anteriorly by the pericardium/chest wall, on the right by the RA/pericardium/lung, on the left by the LV, and posteriorly by the RA/LVOT/LA. The RV ends inferiorly a slice below where the blood is no longer visualized. The superior border is continuous with the PT, ending where the RV appears circular and constant in shape, roughly at the superior extent of the LV and LVOT contour.

Right atrium: The right most chamber of the heart. Bounded anteriorly by the RV, on the right by the LA/pericardium/lung, on the left by

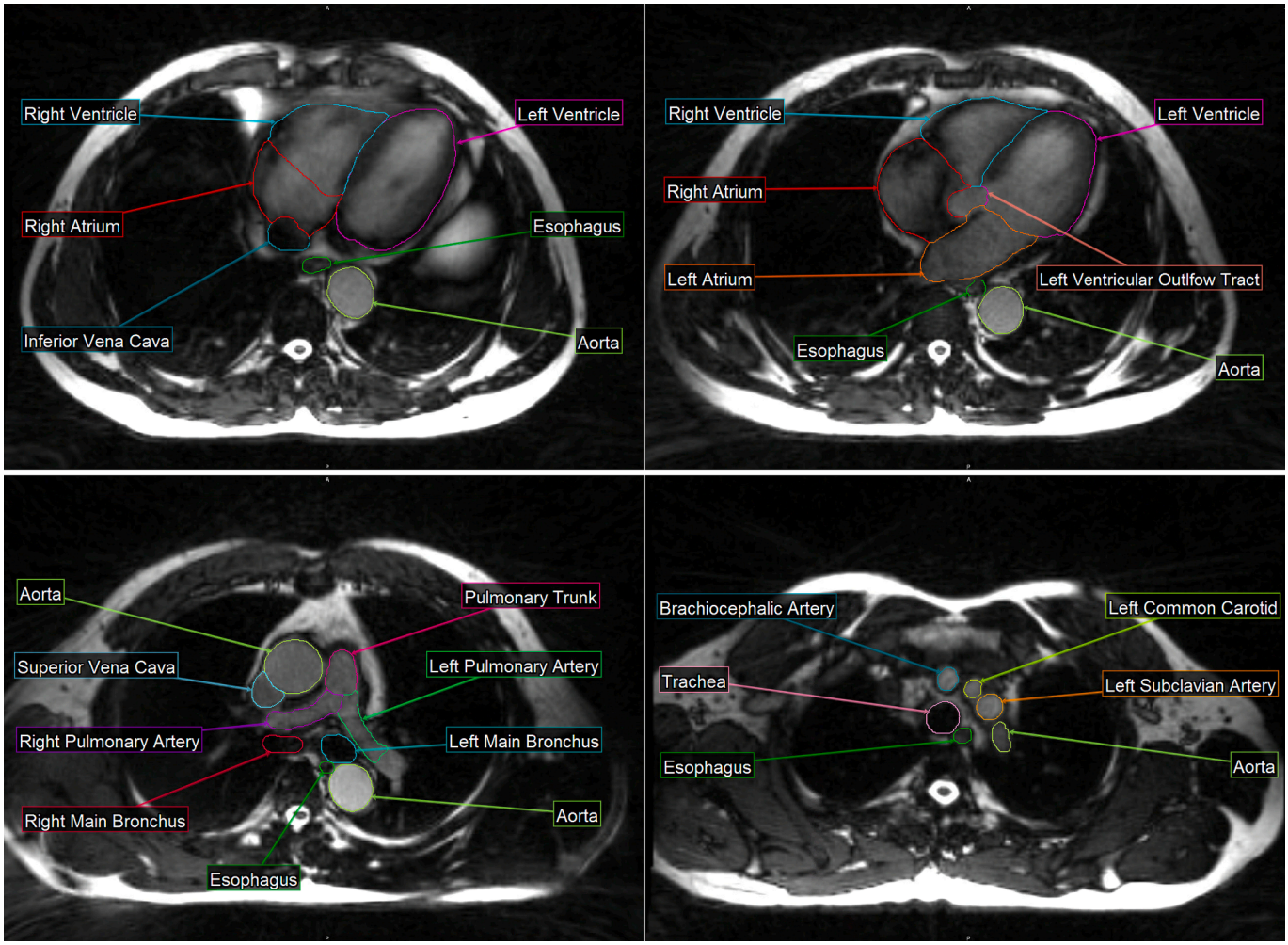

Fig. 1. Representative, ascending, axial 3D bSSFP slices from one volunteer with key cardiac structures contoured and labeled.

the LVOT/LV, and posteriorly by the IVC/LA. The distinction between the RA and RV is essentially a continuation of the line used to divide the LA and LV, from the anterior right most portion of the LVOT to the myocardium. Though not seen, this line is where the tricuspid valve sits. Superiorly and inferiorly the RA ends a slice above and below where the blood is no longer visualized.

3.3. Contouring guidelines – Vasculature

Superior vena cava (SVC): Begin superiorly with the junction of the right and left brachiocephalic veins, then continue inferiorly until the RA is encompassed.

Inferior vena cava: Begin inferior and posterior to the RA, at the bottom of the RA, then extend superiorly until encompassing the RA, with which it is continuous. The inferior extent should extend at least one cm inferior to the chambers.

Aorta: Begin with the slice above the LVOT, as a continuation of this structure. Also contour the descending aorta, the large artery lateral to the spinal column. Follow these superiorly until they join. The inferior extent of the descending aorta should extend at least one cm inferior to the chambers.

Pulmonary trunk: Begin at the slice above the RV and ascend until it bifurcates into the right and left pulmonary arteries.

Left pulmonary artery: Begin at the PT, continue contouring until the structure bifurcates.

Right pulmonary artery: Begin at the PT, continue contouring until the structure bifurcates.

Brachiocephalic artery: The 1st, most anterior vessel coming superiorly off of the aortic arch. The artery will quickly move to the right and end with its bifurcation into the right common carotid and right subclavian arteries.

Left common carotid artery: The 2nd, middle vessel coming superiorly off of the aortic arch. Follow superiorly for one cm above the superior extent of the aorta contour.

Left subclavian artery: The 3rd, most posterior vessel coming superiorly off of the aortic arch. Follow superiorly for one cm above the superior extent of the aorta contour.

Pulmonary veins: The four PVs arise from the posterior, most lateral corners of the LA superiorly and inferiorly on each side and are not always distinguishable using these MRL sequences.

3.4. Contouring guidelines – Respiratory structures and esophagus

Trachea: Central structure with no signal, located posterior to the ascending aorta. Begin contour one cm superior to the aortic arch.

Left main bronchus: Inferior continuation of the trachea at the bifurcation on the left, until it splits further.

Right main bronchus: Inferior continuation of the trachea at the bifurcation on the right, until it splits further.

Esophagus: Hypointense, sometimes air filled structure anterior to the aorta/spinal column and posterior to the ascending aorta/aortic arch/trachea/left bronchus/LA.

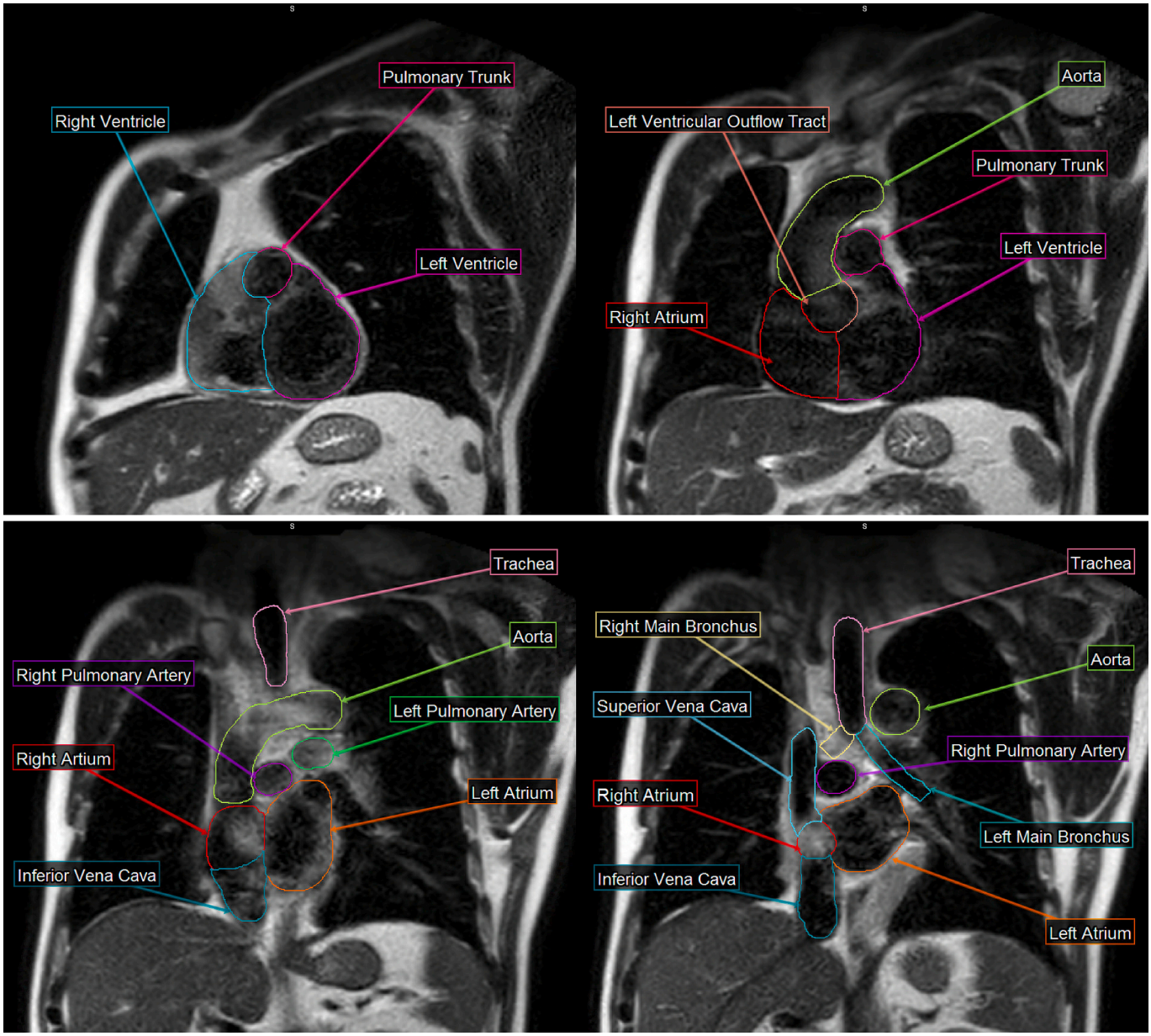

Fig. 2. Representative, ascending, short axis HASTE slices from one volunteer with key cardiac structures contoured and labeled.

3.5. *Contouring guidelines – Conduction system*

Sinoatrial node: The sinoatrial (SA) node is located in the roof of the RA at the approximate junction of the SVC, the right atrial appendage, and the sulcus terminalis. It is one mm below the epicardium, one-two cm long, and roughly 0.5 cm thick. The SA node has automaticity and initiates the cardiac action potential, with its rate augmented by the autonomic nervous system [37]. Start one slice below the SVC contour, just before it becomes distinct from the RA. Contour the SA node one-two cm in the anterior-posterior dimension, and 0.5 cm in the left–-right dimension, within the RA, such that the posterior edge of the contour aligns with the aorta, and the anterior edge of the contour aligns with a line drawn from left to right from the center of the aorta. The right edge of the contour should contact the right edge of the RA.

Internodal pathways: The SA and atrioventricular (AV) nodes are connected through the anterior, middle, and posterior internodal tracts which run through the walls of the RA to the AV node. The anterior internodal tract runs between the RA and the LVOT to the AV node. The middle internodal tract is actually the most posterior when looking at axial slices and runs between the RA and LA to the AV node. The posterior internodal tract is the most lateral, and can be drawn by keeping the cursor in the same location moving inferiorly from the SA node until the RA contour ends, then curving back upwards to the AV node. It passes through the crista terminalis and Eustachian valve to the AV node. Bachmans bundle bifurcates off of the anterior intermodal tract almost immediately. Contour by moving superiorly to the slice with the SVC, extending the contour posterior to the SVC and aorta, and then to the superior LA. [38].

Atrioventricular node: Located in the floor of the RA, in the triangle of Koch, bounded by the interventricular septum, coronary sinus, tricuspid valve annulus, and tendon of Todaro. The AV node relays the signal from the atria to the ventricles, delaying the impulse in order to coordinate atrial and ventricular contraction [39]. It can be approximated within the interventricular septum, a slice or two inferior to the inferior extent of the LVOT, as the abutment of the contours of the LV and RV where they end posteriorly.

Bundle of His: Largely located within the interventricular septum. The right and left bundles are within the right and left most aspects of

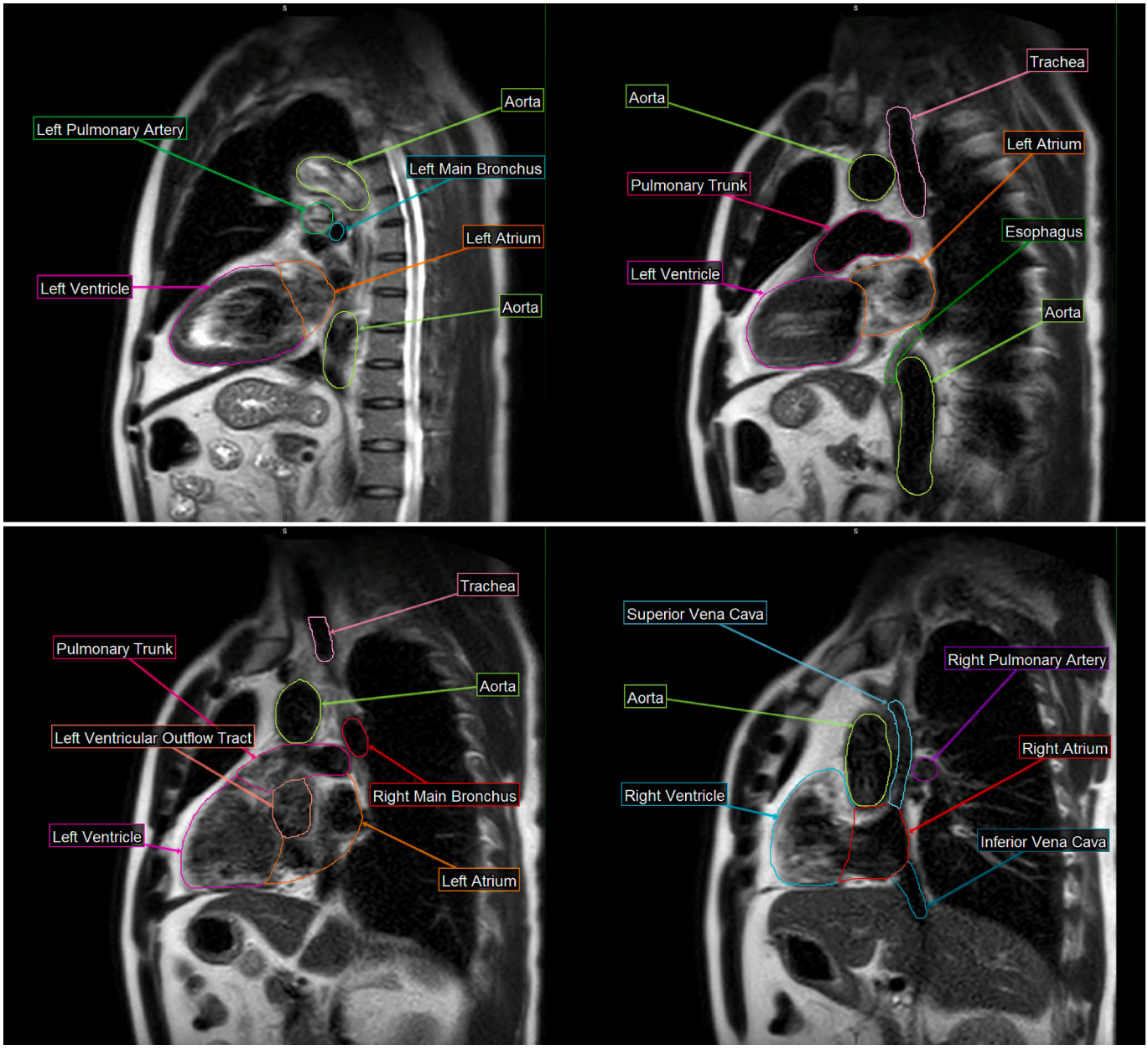

Fig. 3. Representative, ascending, vertical long axis HASTE slices from one volunteer with key cardiac structures contoured and labeled.

the interventricular septum, as it moves toward the apex. The posterior bundle moves inferiorly and then laterally around the LV.

3.6. Volumes

The volumes of relevant cardiac substructures are reported in Table 1. Overall, there was reasonable variation of contour volume across volunteers, consistent with variations in volunteer anatomy. Structures were more easily and clearly delineated on the 3D bSSFP acquired images, owing to improved spatial resolution.

4. Discussion

There have been several cardiac atlases informing our MRL based contours. Feng et al. provided one of the most cited CT based cardiac atlases standardizing heart contours across radiation oncology [30]. A contouring goal is auto segmentation to reduce contouring time and interoperator variability. Zhou et al. contoured contrast enhanced images based on the Feng atlas and used deformable registration techniques to a multi atlas software to auto contour 15 cardiac substructures for use on non-contrast images [36]. Haq et al created a neural network capable of auto segmentation from patients contoured based on the Feng atlas for ten cardiac substructures [40]. The validated atlas shows minimal difference in volume between auto and manual contours, providing the benefit of dose calculations to these substructures [41]. Our atlas could be used in a similar fashion to inform an auto segmentation process on the MRL to augment real time plan adaptation. Cardiac atlases have also been generated for the conduction cycle, valves, and vasculature. Loap et al. generated two cm diameter spheres corresponding to the SA and AV nodes as a novel part of their consensus contouring guidelines [31]. Stockinger et al. developed a retrospective atlas with seven structures, including geometrical surrogate volumes for valve contours, intended for further dose response research [35]. Socha et al. similarly used Feng's atlas along with echocardiograph correlates to better delineate valves [34]. Morris et al. developed a hybrid CT/MR atlas, registering MR findings to CT for CT based planning [33]. Duane

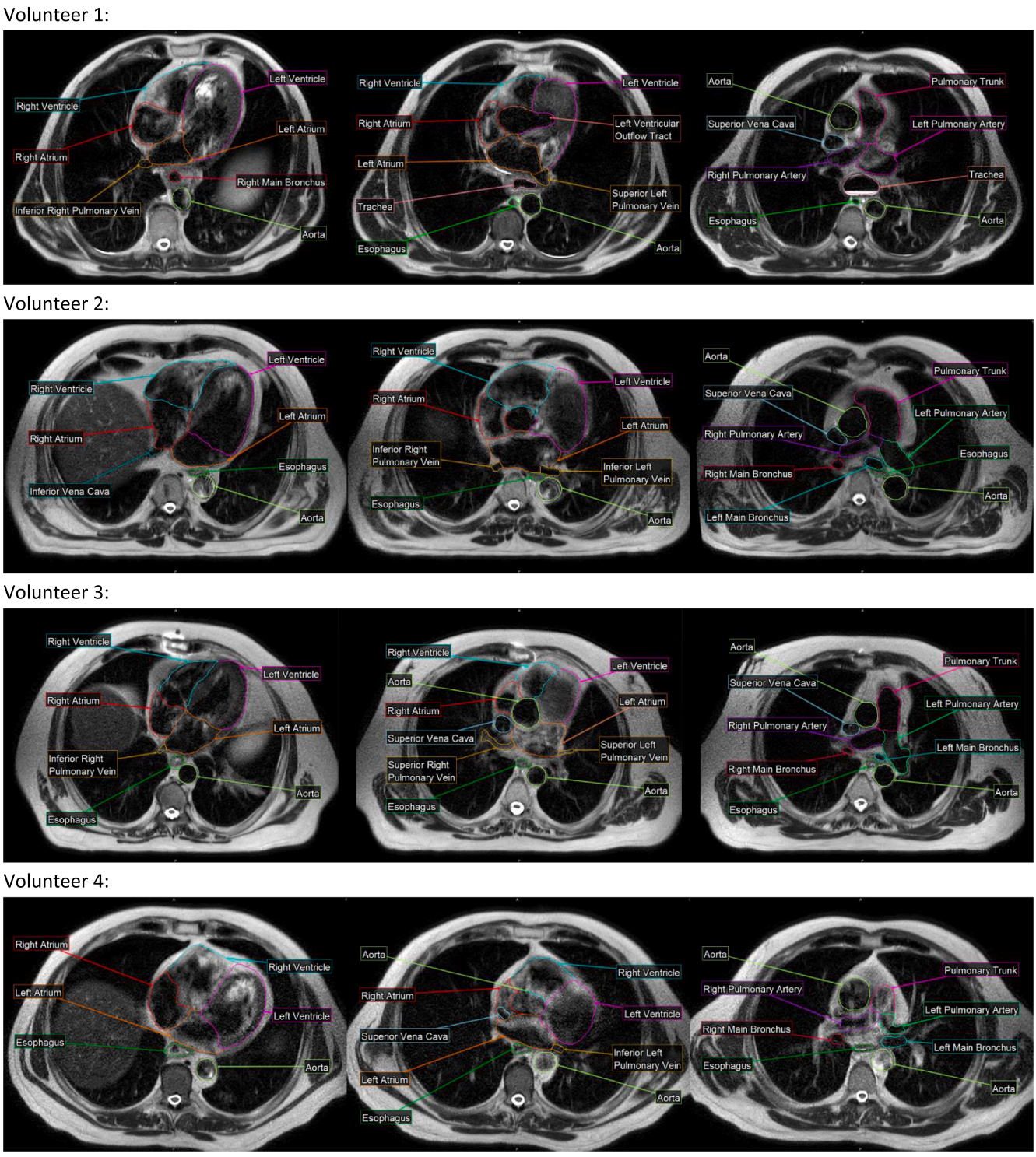

Fig. 4. Representative, ascending slices acquired from four volunteers at similar levels through the heart, delineating slight variations in normal anatomy.

et al. generated an atlas focusing on LV segmentation generating five key segments, from the traditional 17 segment model, to consider effects of dose to different regions of the LV and promote consistent reporting of cardiac doses in radiotherapy. They also describe contouring of key vasculature [29]. Milo et al. developed a comprehensive multidisciplinary cardiac atlas for thoracic radiation oncology with detailed delineation of LV segmentation [32]. Contouring of cardiac substructures and LV segmentation could be applied to the MRL for future dosimetric studies, similar to the ACCOLADE trial.

Our atlas has a number of strengths and novel features. The atlas was developed by and for radiation oncologists, specifically for cardiac ablation and treating thoracic tumors on the MRL, and is the first atlas generated prospectively on 1.5 T MRL to inform adaptive planning rather than CT based planning. These contours may improve cardiac avoidance during MRL treatment for thoracic and breast cancers. We provide instructions for contouring cardiac substructures and the conduction cycle, which in future can be used to estimate dosimetric constraints, inform cardiac sparing techniques, and promote further radiation research on arrhythmias and conduction disorders. Future directions include further optimization of MRL sequences for CMR, use

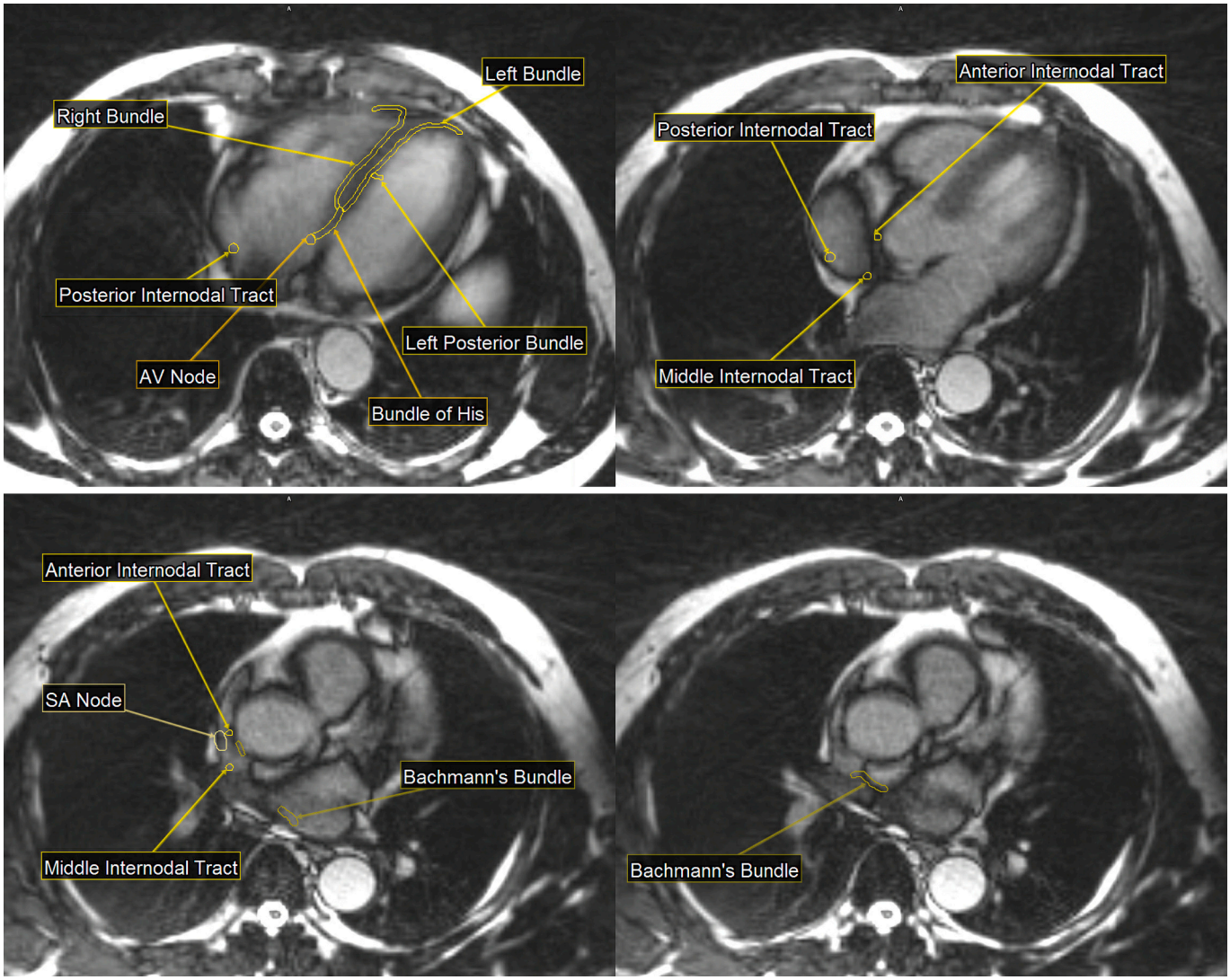

Fig. 5. Representative, axial 3D bSSFP slices with the cardiac conduction system from one volunteer contoured and labeled.

Table 1
Contour Volumes.

HASTE and 3D bSSFP Contour Volume (cc)							
Chambers:	**HASTE 1**	**HASTE 2**	**HASTE 3**	**HASTE 4**	**bSSFP**	**Mean**	**SD**
Left ventricle	270.58	325.65	272.05	254.18	221.35	268.76	37.79
Ventricular outflow tract	13.21	10.44	6.08	9.24	19.52	11.70	5.07
Left atrium	66.08	97.38	89.16	112.45	86.05	90.22	16.93
Right ventricle	158.43	229.48	109.04	222.39	128.53	169.57	54.43
Right atrium	61.18	86.43	72.08	85.13	94.45	79.85	13.17
HASTE and 3D bSSFP Contour Volume (cc)							
Vasculature:	**HASTE 1**	**HASTE 2**	**HASTE 3**	**HASTE 4**	**bSSFP**	**Mean**	**SD**
Superior vena cava	9.36	4.01	14.76	10.36	13.27	10.35	4.16
Inferior vena cava	11.51	9.68	13.72	13.64	11.55	12.02	1.69
Aorta	71.36	89.24	126.93	131.31	185.24	120.82	43.99
Pulmonary trunk	16.48	37.38	36.4	35.86	22.99	29.82	9.51
Left pulmonary artery	10.68	7.61	15.76	17.8	11.75	12.72	4.07
Right pulmonary artery	6.4	18.57	24.13	28.05	15.26	18.48	8.36
HASTE and 3D bSSFP Contour Volume (cc)							
Respiratory Structures	**HASTE 1**	**HASTE 2**	**HASTE 3**	**HASTE 4**	**bSSFP**	**Mean**	**SD**
Trachea	18.87				19.78	19.33	0.64
Left main bronchus	1.26	4.63	2.22	5.07	4.97	3.63	1.77
Right main bronchus	1.56	1.55	2.38	3.89	4.35	2.75	1.31
Pulmonary veins		5.6	4.39	3.21	2.28	3.87	1.44

of functional techniques and inclusion of cardiac and respiratory gating.

While our atlas forms a foundation for further investigation, there are several limitations. We provide two common sequences, but there are other CMR sequences not yet optimized on the MRL (e.g. T2-weighted short-tau inversion recovery, fat suppression, dual inversion recovery, arterial spin labeling, T1 mapping, DWI, phase-contrast velocity mapping, and contrast enhanced sequences) [8,9]. The provided sequences cannot resolve finer vessels, such as the coronary arteries, or the conduction system directly, and are sometimes limited by signal drop out. While the MRL has the technical ability to acquire diagnostic quality images, sequences in this publication do not have cardiac gating, are not as optimized for heart imaging as diagnostic CMR images, and are obtained on 1.5 T rather than 3 T like most modern diagnostic scanners. Furthermore, this atlas was generated by collaborators at one institution, and interobserver agreement was not compared to previous atlases. Finally, healthy volunteers were used rather than patients with known heart pathology, such as those undergoing cardiac ablation, which may complicate contouring. In the future, there is tremendous potential for multiparametric image generation (e.g. function, blood flow, and perfusion) which, once optimized for MRL, would provide exciting new opportunities to study effects of radiation on heart function.

We present the first comprehensive 1.5 T MRL cardiac atlas for radiation oncologists, with a special focus on understanding CMR, cardiac substructures, and the conduction system of the heart. Our atlas can be used to promote dosimetric analysis of radiation toxicity to cardiac and conduction substructures, inform auto segmentation workflows on the MRL, and be integrated into protocols for image registration to improve future adaptive radiotherapy techniques and toxicity research.

CRediT authorship contribution statement

Aronne M. Schottstaedt: Methodology, Visualization, Writing – review & editing. **Eric S. Paulson:** Methodology, Writing – review & editing. **Jason C. Rubenstein:** Writing – review & editing. **Xinfeng Chen:** Methodology. **Eenas A. Omari:** Writing – review & editing. **X Allen Li:** Writing – review & editing. **Chris J. Schultz:** Writing – review & editing. **Lindsay L. Puckett:** Writing – review & editing. **Clifford G. Robinson:** Writing – review & editing. **Filippo Alongi:** Writing – review & editing. **Elizabeth M. Gore:** Writing – review & editing. **William A. Hall:** Conceptualization, Writing – review & editing.

Declaration of competing interest

The authors declare the following financial interests/personal relationships which may be considered as potential competing interests: X Allen Li: Grant/contracts – NIH/NCI, Elekta AB, Siemens; Honorarium – Accuray Inc; Support for meeting – Elekta AB. Fillipo Alongi: Grant/contracts, consulting fees, payment/honorarium, and meeting support – Elekta. Erick Paulson: Grant: Elekta, Siemens; Software licenses – Philips. Christopher Schultz: Grants/Contracts – MRL Consortium; Support for meeting – Elekta. Clifford Robinson: Grants – Varian, Merck; Consulting fees – Varian, radialogica, AstraZeneca, EMD Serono; Stock – Radialogica. Lindsay L. Puckett: Payment/honoraria and support for meeting – Accuray. William Hall: Support for meeting – Elekta. Xinfeng Chen: None. Eenas Omari: None. Elizabeth Gore: None. Aronne Schottstaedt: None.

Appendix A. Supplementary data

Supplementary data to this article can be found online at https://doi.org/10.1016/j.phro.2023.100504.

References

[1] Banfill K, Giuliani M, Aznar M, Franks K, McWilliam A, Schmitt M, et al. Cardiac Toxicity of Thoracic Radiotherapy: Existing Evidence and Future Directions. J Thorac Oncol 2021;16:216–27. https://doi.org/10.1016/j.jtho.2020.11.002.

[2] Yu C, Pathan F, Tan TC, Negishi K. The Utility of Advanced Cardiovascular Imaging in Cancer Patients-When, Why, How, and the Latest Developments. Front Cardiovasc Med 2021;8:728215. https://doi.org/10.3389/fcvm.2021.728215.

[3] Cuculich PS, Schill MR, Kashani R, Mutic S, Lang A, Cooper D, et al. Noninvasive Cardiac Radiation for Ablation of Ventricular Tachycardia. N Engl J Med 2017;377:2325–36. https://doi.org/10.1056/NEJMoa1613773.

[4] Robinson CG, Samson PP, Moore KMS, Hugo GD, Knutson N, Mutic S, et al. Phase I/II Trial of Electrophysiology-Guided Noninvasive Cardiac Radioablation for Ventricular Tachycardia. Circulation 2019;139:313–21. https://doi.org/10.1161/circulationaha.118.038261.

[5] Hall WA, Paulson ES, van der Heide UA, Fuller CD, Raaymakers BW, Lagendijk JJW, et al. The transformation of radiation oncology using real-time magnetic resonance guidance: A review. Eur J Cancer 2019;122:42–52. https://doi.org/10.1016/j.ejca.2019.07.021.

[6] Tseng WY, Su MY, Tseng YH. Introduction to Cardiovascular Magnetic Resonance: Technical Principles and Clinical Applications. Acta Cardiol Sin 2016;32:129–44. https://doi.org/10.6515/acs20150616a.

[7] Ginat DT, Fong MW, Tuttle DJ, Hobbs SK, Vyas RC. Cardiac imaging: Part 1, MR pulse sequences, imaging planes, and basic anatomy. AJR Am J Roentgenol 2011;197:808–15. https://doi.org/10.2214/ajr.10.7231.

[8] Krishnamurthy R, Cheong B, Muthupillai R. Tools for cardiovascular magnetic resonance imaging. Cardiovasc Diagn Ther 2014;4:104–25. https://doi.org/10.3978/j.issn.2223-3652.2014.03.06.

[9] Saeed M, Van TA, Krug R, Hetts SW, Wilson MW. Cardiac MR imaging: current status and future direction. Cardiovasc Diagn Ther 2015;5:290–310. https://doi.org/10.3978/j.issn.2223-3652.2015.06.07.

[10] Thimmappa ND, Cooper MA, Nguyen TD, Dutruel SP, Kawaji K, Weinsaft JW. Electrocardiographic Pad for Efficient Cardiac MR Gating. Radiology 2016;278:578–84. https://doi.org/10.1148/radiol.2015142318.

[11] Akdag O, Borman PTS, Woodhead P, Uijtewaal P, Mandija S, Van Asselen B, et al. First experimental exploration of real-time cardiorespiratory motion management for future stereotactic arrhythmia radioablation treatments on the MR-linac. Phys Med Biol 2022;67. https://doi.org/10.1088/1361-6560/ac5717.

[12] Cerqueira MD, Weissman NJ, Dilsizian V, Jacobs AK, Kaul S, Laskey WK, et al. Standardized myocardial segmentation and nomenclature for tomographic imaging of the heart. A statement for healthcare professionals from the Cardiac Imaging Committee of the Council on Clinical Cardiology of the American Heart Association. Circulation 2002;105:539–42. https://doi.org/10.1161/hc0402.102975.

[13] Darby SC, Ewertz M, McGale P, Bennet AM, Blom-Goldman U, Brønnum D, et al. Risk of ischemic heart disease in women after radiotherapy for breast cancer. N Engl J Med 2013;368:987–98. https://doi.org/10.1056/NEJMoa1209825.

[14] Correa CR, Das IJ, Litt HI, Ferrari V, Hwang WT, Solin LJ, et al. Association between tangential beam treatment parameters and cardiac abnormalities after definitive radiation treatment for left-sided breast cancer. Int J Radiat Oncol Biol Phys 2008;72:508–16. https://doi.org/10.1016/j.ijrobp.2007.12.037.

[15] Correa CR, Litt HI, Hwang WT, Ferrari VA, Solin LJ, Harris EE. Coronary artery findings after left-sided compared with right-sided radiation treatment for early-stage breast cancer. J Clin Oncol 2007;25:3031–7. https://doi.org/10.1200/jco.2006.08.6595.

[16] Cutter DJ, Schaapveld M, Darby SC, Hauptmann M, van Nimwegen FA, Krol AD, et al. Risk of valvular heart disease after treatment for Hodgkin lymphoma. J Natl Cancer Inst 2015;107. https://doi.org/10.1093/jnci/djv008.

[17] Erven K, Jurcut R, Weltens C, Giusca S, Ector J, Wildiers H, et al. Acute radiation effects on cardiac function detected by strain rate imaging in breast cancer patients. Int J Radiat Oncol Biol Phys 2011;79:1444–51. https://doi.org/10.1016/j.ijrobp.2010.01.004.

[18] Gagliardi G, Constine LS, Moiseenko V, Correa C, Pierce LJ, Allen AM, et al. Radiation dose-volume effects in the heart. Int J Radiat Oncol Biol Phys 2010;76:S77–85. https://doi.org/10.1016/j.ijrobp.2009.04.093.

[19] Maraldo MV, Brodin NP, Vogelius IR, Aznar MC, Munck Af Rosenschöld P, Petersen PM, et al. Risk of developing cardiovascular disease after involved node radiotherapy versus mantle field for Hodgkin lymphoma. Int J Radiat Oncol Biol Phys 2012;83:1232–7. https://doi.org/10.1016/j.ijrobp.2011.09.020.

[20] Moignier A, Broggio D, Derreumaux S, Beaudré A, Girinsky T, Paul JF, et al. Coronary stenosis risk analysis following Hodgkin lymphoma radiotherapy: A study based on patient specific artery segments dose calculation. Radiother Oncol 2015;117:467–72. https://doi.org/10.1016/j.radonc.2015.07.043.

[21] Nilsson G, Holmberg L, Garmo H, Duvernoy O, Sjögren I, Lagerqvist B, et al. Distribution of coronary artery stenosis after radiation for breast cancer. J Clin Oncol 2012;30:380–6. https://doi.org/10.1200/jco.2011.34.5900.

[22] Yegya-Raman N, Wang K, Kim S, Reyhan M, Deek MP, Sayan M, et al. Dosimetric Predictors of Symptomatic Cardiac Events After Conventional-Dose Chemoradiation Therapy for Inoperable NSCLC. J Thorac Oncol 2018;13:1508–18. https://doi.org/10.1016/j.jtho.2018.05.028.

[23] Wang K, Pearlstein KA, Patchett ND, Deal AM, Mavroidis P, Jensen BC, et al. Heart dosimetric analysis of three types of cardiac toxicity in patients treated on dose-escalation trials for Stage III non-small-cell lung cancer. Radiother Oncol 2017;125:293–300. https://doi.org/10.1016/j.radonc.2017.10.001.

[24] Vivekanandan S, Landau DB, Counsell N, Warren DR, Khwanda A, Rosen SD, et al. The Impact of Cardiac Radiation Dosimetry on Survival After Radiation Therapy

for Non-Small Cell Lung Cancer. Int J Radiation Oncology Biol Phys 2017;99: 51–60. https://doi.org/10.1016/j.ijrobp.2017.04.026.
[25] Atkins KM, Chaunzwa TL, Lamba N, Bitterman DS, Rawal B, Bredfeldt J, et al. Association of Left Anterior Descending Coronary Artery Radiation Dose With Major Adverse Cardiac Events and Mortality in Patients With Non-Small Cell Lung Cancer. JAMA Oncol 2021;7:206–19. https://doi.org/10.1001/jamaoncol.2020.6332.
[26] Craddock M, Nestle U, Koenig J, Schimek-Jasch T, Kremp S, Lenz S, et al. Cardiac Function Modifies the Impact of Heart Base Dose on Survival: A Voxel-Wise Analysis of Patients With Lung Cancer From the PET-Plan Trial. J Thorac Oncol 2023;18:57–66. https://doi.org/10.1016/j.jtho.2022.09.004.
[27] Banfill K, Sun F, Mcwilliam A, Abravan A, Lilley J, Wheller R, et al. Avoiding cardiac toxicity in patients undergoing curative intent radiotherapy for lung cancer. Lung Cancer 2019;127. https://doi.org/10.1016/s0169-5002(19)30263-6.
[28] Iaizzo PA. University of minnesota: Atlas of human cardiac anatomy, the visible heart laboratory. Accessed 5/3/2023, 2023. http://www.vhlab.umn.edu/atlas/static-mri/short-axis-valve/index.shtml.
[29] Duane F, Aznar MC, Bartlett F, Cutter DJ, Darby SC, Jagsi R, et al. A cardiac contouring atlas for radiotherapy. Radiother Oncol 2017;122:416–22. https://doi.org/10.1016/j.radonc.2017.01.008.
[30] Feng M, Moran JM, Koelling T, Chughtai A, Chan JL, Freedman L, et al. Development and validation of a heart atlas to study cardiac exposure to radiation following treatment for breast cancer. Int J Radiat Oncol Biol Phys 2011;79:10–8. https://doi.org/10.1016/j.ijrobp.2009.10.058.
[31] Loap P, Servois V, Dhonneur G, Kirov K, Fourquet A, Kirova Y. A Radiation Therapy Contouring Atlas for Cardiac Conduction Node Delineation. Pract Radiat Oncol 2021;11:e434–7. https://doi.org/10.1016/j.prro.2021.02.002.
[32] Milo MLH, Offersen BV, Bechmann T, Diederichsen ACP, Hansen CR, Holtved E, et al. Delineation of whole heart and substructures in thoracic radiation therapy: National guidelines and contouring atlas by the Danish Multidisciplinary Cancer Groups. Radiother Oncol 2020;150:121–7. https://doi.org/10.1016/j.radonc.2020.06.015.
[33] Morris ED, Ghanem AI, Pantelic MV, Walker EM, Han X, Glide-Hurst CK. Cardiac Substructure Segmentation and Dosimetry Using a Novel Hybrid Magnetic Resonance and Computed Tomography Cardiac Atlas. Int J Radiat Oncol Biol Phys 2019;103:985–93. https://doi.org/10.1016/j.ijrobp.2018.11.025.
[34] Socha J, Rygielska A, Uziębło-Życzkowska B, Chałubińska-Fendler J, Jurek A, Maciorowska M, et al. Contouring cardiac substructures on average intensity projection 4D-CT for lung cancer radiotherapy: A proposal of a heart valve contouring atlas. Radiother Oncol 2022;167:261–8. https://doi.org/10.1016/j.radonc.2021.12.041.
[35] Stockinger M, Karle H, Rennau H, Sebb S, Wolf U, Remmele J, et al. Heart atlas for retrospective cardiac dosimetry: a multi-institutional study on interobserver contouring variations and their dosimetric impact. Radiat Oncol 2021;16:241. https://doi.org/10.1186/s13014-021-01965-5.
[36] Zhou R, Liao Z, Pan T, Milgrom SA, Pinnix CC, Shi A, et al. Cardiac atlas development and validation for automatic segmentation of cardiac substructures. Radiother Oncol 2017;122:66–71. https://doi.org/10.1016/j.radonc.2016.11.016.
[37] Kennedy A, Finlay DD, Guldenring D, Bond R, Moran K, McLaughlin J. The Cardiac Conduction System: Generation and Conduction of the Cardiac Impulse. Crit Care Nurs Clin North Am 2016;28:269–79. https://doi.org/10.1016/j.cnc.2016.04.001.
[38] Paul A. Iaizzo. University of minnesota: Atlas of human cardiac anatomy, the visible heart laboratory. http://www.vhlab.umn.edu/atlas/static-mri/short-axis-valve/index.shtml.
[39] Liddy S, McQuade C, Walsh KP, Loo B, Buckley O. The Assessment of Cardiac Masses by Cardiac CT and CMR Including Pre-op 3D Reconstruction and Planning. Curr Cardiol Rep 2019;21:103. https://doi.org/10.1007/s11886-019-1196-7.
[40] Haq R, Hotca A, Apte A, Rimner A, Deasy JO, Thor M. Cardio-pulmonary substructure segmentation of radiotherapy computed tomography images using convolutional neural networks for clinical outcomes analysis. Phys Imaging Radiation Oncol 2020;14:61–6. https://doi.org/10.1016/j.phro.2020.05.009.
[41] Walls GM, Giacometti V, Apte A, Thor M, McCann C, Hanna GG, et al. Validation of an established deep learning auto-segmentation tool for cardiac substructures in 4D radiotherapy planning scans. Phys Imaging Radiation Oncol 2022;23:118–26. https://doi.org/10.1016/j.phro.2022.07.003.